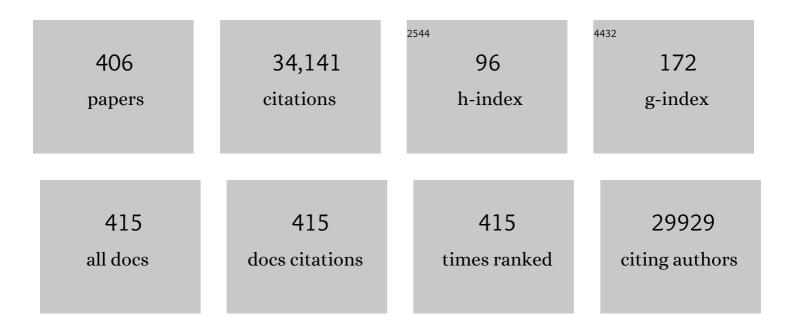
List of Publications by Year in descending order

Source: https://exaly.com/author-pdf/7606608/publications.pdf Version: 2024-02-01



ΙΠΝΕΛ ΖΗΙ

#	Article	IF	CITATIONS
1	Single Cobalt Atoms with Precise Nâ€Coordination as Superior Oxygen Reduction Reaction Catalysts. Angewandte Chemie - International Edition, 2016, 55, 10800-10805.	13.8	1,836
2	Selective visible-light-driven photocatalytic CO2 reduction to CH4 mediated by atomically thin CuIn5S8 layers. Nature Energy, 2019, 4, 690-699.	39.5	948
3	Oxide Defect Engineering Enables to Couple Solar Energy into Oxygen Activation. Journal of the American Chemical Society, 2016, 138, 8928-8935.	13.7	840
4	Tailoring the dâ€Band Centers Enables Co ₄ N Nanosheets To Be Highly Active for Hydrogen Evolution Catalysis. Angewandte Chemie - International Edition, 2018, 57, 5076-5080.	13.8	728
5	Exclusive Ni–N ₄ Sites Realize Near-Unity CO Selectivity for Electrochemical CO ₂ Reduction. Journal of the American Chemical Society, 2017, 139, 14889-14892.	13.7	725
6	Refining Defect States in W ₁₈ O ₄₉ by Mo Doping: A Strategy for Tuning N ₂ Activation towards Solar-Driven Nitrogen Fixation. Journal of the American Chemical Society, 2018, 140, 9434-9443.	13.7	722
7	Heterogeneous Single-Atom Photocatalysts: Fundamentals and Applications. Chemical Reviews, 2020, 120, 12175-12216.	47.7	620
8	Synergetic interaction between neighbouring platinum monomers in CO2 hydrogenation. Nature Nanotechnology, 2018, 13, 411-417.	31.5	584
9	Fabrication of composite photocatalyst g-C3N4–ZnO and enhancement of photocatalytic activity under visible light. Dalton Transactions, 2012, 41, 6756.	3.3	553
10	Enhancing CO ₂ Electroreduction with the Metal–Oxide Interface. Journal of the American Chemical Society, 2017, 139, 5652-5655.	13.7	468
11	Thiol-functionalization of metal-organic framework by a facile coordination-based postsynthetic strategy and enhanced removal of Hg2+ from water. Journal of Hazardous Materials, 2011, 196, 36-43.	12.4	456
12	Isolation of Cu Atoms in Pd Lattice: Forming Highly Selective Sites for Photocatalytic Conversion of CO ₂ to CH ₄ . Journal of the American Chemical Society, 2017, 139, 4486-4492.	13.7	455
13	Highly Active and Stable Metal Single-Atom Catalysts Achieved by Strong Electronic Metal–Support Interactions. Journal of the American Chemical Society, 2019, 141, 14515-14519.	13.7	455
14	Enabling unassisted solar water splitting by iron oxide and silicon. Nature Communications, 2015, 6, 7447.	12.8	429
15	Scaledâ€Up Synthesis of Amorphous NiFeMo Oxides and Their Rapid Surface Reconstruction for Superior Oxygen Evolution Catalysis. Angewandte Chemie - International Edition, 2019, 58, 15772-15777.	13.8	426
16	New photocatalysts based on MIL-53 metal–organic frameworks for the decolorization of methylene blue dye. Journal of Hazardous Materials, 2011, 190, 945-951.	12.4	416
17	Low-Cost Synthesis of Flowerlike α-Fe ₂ O ₃ Nanostructures for Heavy Metal Ion Removal: Adsorption Property and Mechanism. Langmuir, 2012, 28, 4573-4579.	3.5	409
18	Protecting Copper Oxidation State via Intermediate Confinement for Selective CO ₂ Electroreduction to C ₂₊ Fuels. Journal of the American Chemical Society, 2020, 142, 6400-6408.	13.7	396

#	Article	IF	CITATIONS
19	Heterogeneous Singleâ€Atom Catalyst for Visibleâ€Lightâ€Driven Highâ€Turnover CO ₂ Reduction: The Role of Electron Transfer. Advanced Materials, 2018, 30, e1704624.	21.0	383
20	Single Cobalt Atoms with Precise Nâ€Coordination as Superior Oxygen Reduction Reaction Catalysts. Angewandte Chemie, 2016, 128, 10958-10963.	2.0	373
21	Partially Oxidized SnS ₂ Atomic Layers Achieving Efficient Visible-Light-Driven CO ₂ Reduction. Journal of the American Chemical Society, 2017, 139, 18044-18051.	13.7	368
22	Doping-induced structural phase transition in cobalt diselenide enables enhanced hydrogen evolution catalysis. Nature Communications, 2018, 9, 2533.	12.8	356
23	Precisely Tuning the Number of Fe Atoms in Clusters on N-Doped Carbon toward Acidic Oxygen Reduction Reaction. CheM, 2019, 5, 2865-2878.	11.7	346
24	Facile fabrication of magnetic metal–organic framework nanocomposites for potential targeted drug delivery. Journal of Materials Chemistry, 2011, 21, 3843.	6.7	343
25	Sulfur-anchoring synthesis of platinum intermetallic nanoparticle catalysts for fuel cells. Science, 2021, 374, 459-464.	12.6	343
26	Tuning orbital orientation endows molybdenum disulfide with exceptional alkaline hydrogen evolution capability. Nature Communications, 2019, 10, 1217.	12.8	322
27	Design and Epitaxial Growth of MoSe ₂ –NiSe Vertical Heteronanostructures with Electronic Modulation for Enhanced Hydrogen Evolution Reaction. Chemistry of Materials, 2016, 28, 1838-1846.	6.7	310
28	Electronic structure and chemical bonding of a graphene oxide–sulfur nanocomposite for use in superior performance lithium–sulfur cells. Physical Chemistry Chemical Physics, 2012, 14, 13670.	2.8	305
29	A Janus Nickel Cobalt Phosphide Catalyst for Highâ€Efficiency Neutralâ€pH Water Splitting. Angewandte Chemie - International Edition, 2018, 57, 15445-15449.	13.8	299
30	Fe3O4@MOF core–shell magnetic microspheres with a designable metal–organic framework shell. Journal of Materials Chemistry, 2012, 22, 9497.	6.7	285
31	Atomic-level insights in optimizing reaction paths for hydroformylation reaction over Rh/CoO single-atom catalyst. Nature Communications, 2016, 7, 14036.	12.8	281
32	Surface-Catalyzed C–C Covalent Coupling Strategies toward the Synthesis of Low-Dimensional Carbon-Based Nanostructures. Accounts of Chemical Research, 2015, 48, 2484-2494.	15.6	273
33	Implementing Metalâ€toâ€Ligand Charge Transfer in Organic Semiconductor for Improved Visibleâ€Nearâ€Infrared Photocatalysis. Advanced Materials, 2016, 28, 6959-6965.	21.0	268
34	Enabling Visibleâ€Lightâ€Driven Selective CO ₂ Reduction by Doping Quantum Dots: Trapping Electrons and Suppressing H ₂ Evolution. Angewandte Chemie - International Edition, 2018, 57, 16447-16451.	13.8	262
35	Infrared Light-Driven CO2 Overall Splitting at Room Temperature. Joule, 2018, 2, 1004-1016.	24.0	258
36	Metal–organic frameworks MIL-88A hexagonal microrods as a new photocatalyst for efficient decolorization of methylene blue dye. Dalton Transactions, 2014, 43, 3792-3798.	3.3	231

#	Article	IF	CITATIONS
37	Boosting hydrogen evolution on MoS2 via co-confining selenium in surface and cobalt in inner layer. Nature Communications, 2020, 11, 3315.	12.8	229
38	<i>Acacia Senegal</i> –Inspired Bifunctional Binder for Longevity of Lithium–Sulfur Batteries. Advanced Energy Materials, 2015, 5, 1500878.	19.5	223
39	Oxygen vacancy associated single-electron transfer for photofixation of CO2 to long-chain chemicals. Nature Communications, 2019, 10, 788.	12.8	222
40	Interrelationships among Grain Size, Surface Composition, Air Stability, and Interfacial Resistance of Al-Substituted Li ₇ La ₃ Zr ₂ O ₁₂ Solid Electrolytes. ACS Applied Materials & Interfaces, 2015, 7, 17649-17655.	8.0	220
41	Enhancing both selectivity and coking-resistance of a single-atom Pd1/C3N4 catalyst for acetylene hydrogenation. Nano Research, 2017, 10, 1302-1312.	10.4	220
42	Metal–Organic Framework Coating Enhances the Performance of Cu ₂ O in Photoelectrochemical CO ₂ Reduction. Journal of the American Chemical Society, 2019, 141, 10924-10929.	13.7	219
43	Facile fabrication of magnetically separable graphitic carbon nitride photocatalysts with enhanced photocatalytic activity under visible light. Journal of Materials Chemistry A, 2013, 1, 3008.	10.3	216
44	Carbon Dioxide Electroreduction into Syngas Boosted by a Partially Delocalized Charge in Molybdenum Sulfide Selenide Alloy Monolayers. Angewandte Chemie - International Edition, 2017, 56, 9121-9125.	13.8	205
45	Unconventional CN vacancies suppress iron-leaching in Prussian blue analogue pre-catalyst for boosted oxygen evolution catalysis. Nature Communications, 2019, 10, 2799.	12.8	202
46	Photocatalytic Conversion of Waste Plastics into C ₂ Fuels under Simulated Natural Environment Conditions. Angewandte Chemie - International Edition, 2020, 59, 15497-15501.	13.8	198
47	Bimetallic nickel-molybdenum/tungsten nanoalloys for high-efficiency hydrogen oxidation catalysis in alkaline electrolytes. Nature Communications, 2020, 11, 4789.	12.8	192
48	Disentangling the size-dependent geometric and electronic effects of palladium nanocatalysts beyond selectivity. Science Advances, 2019, 5, eaat6413.	10.3	187
49	Nickel Doping in Atomically Thin Tin Disulfide Nanosheets Enables Highly Efficient CO ₂ Reduction. Angewandte Chemie - International Edition, 2018, 57, 10954-10958.	13.8	186
50	Size-dependent dynamic structures of supported gold nanoparticles in CO oxidation reaction condition. Proceedings of the National Academy of Sciences of the United States of America, 2018, 115, 7700-7705.	7.1	183
51	Integrated Quasiplane Heteronanostructures of MoSe ₂ /Bi ₂ Se ₃ Hexagonal Nanosheets: Synergetic Electrocatalytic Water Splitting and Enhanced Supercapacitor Performance. Advanced Functional Materials, 2017, 27, 1703864.	14.9	170
52	Hierarchically mesostructured MIL-101 metal–organic frameworks: supramolecular template-directed synthesis and accelerated adsorption kinetics for dye removal. CrystEngComm, 2012, 14, 1613-1617.	2.6	169
53	Boosting Water Dissociation Kinetics on Pt–Ni Nanowires by Nâ€Induced Orbital Tuning. Advanced Materials, 2019, 31, e1807780.	21.0	167
54	Surfaceâ€Assisted Organic Synthesis of Hyperbenzene Nanotroughs. Angewandte Chemie - International Edition, 2013, 52, 4668-4672.	13.8	166

#	Article	IF	CITATIONS
55	Nobleâ€Metalâ€Free Janusâ€like Structures by Cation Exchange for Zâ€6cheme Photocatalytic Water Splitting under Broadband Light Irradiation. Angewandte Chemie - International Edition, 2017, 56, 4206-4210.	13.8	166
56	Synergizing metal–support interactions and spatial confinement boosts dynamics of atomic nickel for hydrogenations. Nature Nanotechnology, 2021, 16, 1141-1149.	31.5	165
57	Controlled synthesis of novel Au@MIL-100(Fe) core–shell nanoparticles with enhanced catalytic performance. Chemical Communications, 2013, 49, 1267-1269.	4.1	163
58	Synergy between Palladium Single Atoms and Nanoparticles via Hydrogen Spillover for Enhancing CO ₂ Photoreduction to CH ₄ . Advanced Materials, 2022, 34, e2200057.	21.0	162
59	Structure Sensitivity of Auâ€īiO ₂ Strong Metal–Support Interactions. Angewandte Chemie - International Edition, 2021, 60, 12074-12081.	13.8	161
60	Direct XPS Evidence for Charge Transfer from a Reduced Rutile TiO ₂ (110) Surface to Au Clusters. Journal of Physical Chemistry C, 2007, 111, 12434-12439.	3.1	156
61	Carbon Dioxide Electroreduction into Syngas Boosted by a Partially Delocalized Charge in Molybdenum Sulfide Selenide Alloy Monolayers. Angewandte Chemie, 2017, 129, 9249-9253.	2.0	154
62	Ultrastable and Efficient Visibleâ€lightâ€driven CO ₂ Reduction Triggered by Regenerative Oxygenâ€Vacancies in Bi ₂ O ₂ CO ₃ Nanosheets. Angewandte Chemie - International Edition, 2021, 60, 13840-13846.	13.8	152
63	A Confinement Strategy for Stabilizing ZIFâ€Derived Bifunctional Catalysts as a Benchmark Cathode of Flexible Allâ€Solidâ€State Zinc–Air Batteries. Advanced Materials, 2018, 30, e1805268.	21.0	147
64	Ultrathin Conductor Enabling Efficient IR Light CO ₂ Reduction. Journal of the American Chemical Society, 2019, 141, 423-430.	13.7	146
65	Microwave-assisted synthesis of highly fluorescent nanoparticles of a melamine-based porous covalent organic framework for trace-level detection of nitroaromatic explosives. Journal of Hazardous Materials, 2012, 221-222, 147-154.	12.4	145
66	High urvature Transitionâ€Metal Chalcogenide Nanostructures with a Pronounced Proximity Effect Enable Fast and Selective CO ₂ Electroreduction. Angewandte Chemie - International Edition, 2020, 59, 8706-8712.	13.8	145
67	Microwave-enhanced synthesis of magnetic porous covalent triazine-based framework composites for fast separation of organic dye from aqueous solution. Journal of Hazardous Materials, 2011, 186, 984-990.	12.4	137
68	Direct Observation of Two Electron Holes in a Hematite Photoanode during Photoelectrochemical Water Splitting. Journal of Physical Chemistry C, 2012, 116, 16870-16875.	3.1	137
69	Oxygen vacancy modulated Ti2Nb10O29-x embedded onto porous bacterial cellulose carbon for highly efficient lithium ion storage. Nano Energy, 2019, 58, 355-364.	16.0	137
70	High-performance hybrid oxide catalyst of manganese and cobalt for low-pressure methanol synthesis. Nature Communications, 2015, 6, 6538.	12.8	135
71	Surface-Assisted Formation, Assembly, and Dynamics of Planar Organometallic Macrocycles and Zigzag Shaped Polymer Chains with C–Cu–C Bonds. ACS Nano, 2014, 8, 709-718.	14.6	134
72	Synthesis of Subâ€2â€nm Ironâ€Doped NiSe ₂ Nanowires and Their Surface onfined Oxidation for Oxygen Evolution Catalysis. Angewandte Chemie - International Edition, 2018, 57, 4020-4024.	13.8	133

#	Article	IF	CITATIONS
73	Atomically Dispersed Ru on Ultrathin Pd Nanoribbons. Journal of the American Chemical Society, 2016, 138, 13850-13853.	13.7	132
74	Size-dependent catalytic activity over carbon-supported palladium nanoparticles in dehydrogenation of formic acid. Journal of Catalysis, 2017, 352, 371-381.	6.2	132
75	Multifunctional Au-Fe ₃ O ₄ @MOF core–shell nanocomposite catalysts with controllable reactivity and magnetic recyclability. Nanoscale, 2015, 7, 1201-1208.	5.6	130
76	Asymmetric Triple-Atom Sites Confined in Ternary Oxide Enabling Selective CO ₂ Photothermal Reduction to Acetate. Journal of the American Chemical Society, 2021, 143, 18233-18241.	13.7	130
77	Pt Single Atoms Embedded in the Surface of Ni Nanocrystals as Highly Active Catalysts for Selective Hydrogenation of Nitro Compounds. Nano Letters, 2018, 18, 3785-3791.	9.1	127
78	Perovskite Oxyfluoride Electrode Enabling Direct Electrolyzing Carbon Dioxide with Excellent Electrochemical Performances. Advanced Energy Materials, 2019, 9, 1803156.	19.5	127
79	Impact of the Coordination Environment on Atomically Dispersed Pt Catalysts for Oxygen Reduction Reaction. ACS Catalysis, 2020, 10, 907-913.	11.2	121
80	Optimizing reaction paths for methanol synthesis from CO2 hydrogenation via metal-ligand cooperativity. Nature Communications, 2019, 10, 1885.	12.8	116
81	Facile fabrication of CdS-metal-organic framework nanocomposites with enhanced visible-light photocatalytic activity for organic transformation. Nano Research, 2015, 8, 1834-1846.	10.4	114
82	Kinetic parameters of CO adsorbed on Pt(111) studied by in situ high resolution x-ray photoelectron spectroscopy. Journal of Chemical Physics, 2002, 117, 10852-10859.	3.0	113
83	Synthesis of bipyridine-based covalent organic frameworks for visible-light-driven photocatalytic water oxidation. Applied Catalysis B: Environmental, 2020, 262, 118271.	20.2	113
84	Understanding the degradation mechanism of rechargeable lithium/sulfur cells: a comprehensive study of the sulfur–graphene oxide cathode after discharge–charge cycling. Physical Chemistry Chemical Physics, 2014, 16, 16931-16940.	2.8	112
85	Investigation of surface effects through the application of the functional binders in lithium sulfur batteries. Nano Energy, 2015, 16, 28-37.	16.0	112
86	Fe ₃ O ₄ @MOF core–shell magnetic microspheres as excellent catalysts for the Claisen–Schmidt condensation reaction. Nanoscale, 2014, 6, 1596-1601.	5.6	111
87	Post-combustion CO2 capture with the HKUST-1 and MIL-101(Cr) metal–organic frameworks: Adsorption, separation and regeneration investigations. Microporous and Mesoporous Materials, 2013, 179, 191-197.	4.4	109
88	Efficient Infraredâ€Lightâ€Driven CO ₂ Reduction Over Ultrathin Metallic Niâ€doped CoS ₂ Nanosheets. Angewandte Chemie - International Edition, 2021, 60, 8705-8709.	13.8	108
89	The Effect of Thermal Reduction on the Photoluminescence and Electronic Structures of Graphene Oxides. Scientific Reports, 2014, 4, 4525.	3.3	106
90	Fumarate-based metal-organic frameworks as a new platform for highly selective removal of fluoride from brick tea. Scientific Reports, 2018, 8, 939.	3.3	105

#	Article	IF	CITATIONS
91	Bottom-Up Synthesis of Metalated Carbyne. Journal of the American Chemical Society, 2016, 138, 1106-1109.	13.7	104
92	Suppression of Structural Phase Transition in VO2 by Epitaxial Strain in Vicinity of Metal-insulator Transition. Scientific Reports, 2016, 6, 23119.	3.3	102
93	Phase and Morphology Transformation of MnO ₂ Induced by Ionic Liquids toward Efficient Water Oxidation. ACS Catalysis, 2018, 8, 10137-10147.	11.2	102
94	Direct Synthesis of Nickel(II) Tetraphenylporphyrin and Its Interaction with a Au(111) Surface: A Comprehensive Study. Journal of Physical Chemistry C, 2010, 114, 9908-9916.	3.1	100
95	Highly energy- and time-efficient synthesis of porous triazine-based framework: microwave-enhanced ionothermal polymerization and hydrogen uptake. Journal of Materials Chemistry, 2010, 20, 6413.	6.7	99
96	A Rational Selfâ€Sacrificing Template Route to Metal–Organic Framework Nanotubes and Reversible Vaporâ€Phase Detection of Nitroaromatic Explosives. Small, 2012, 8, 225-230.	10.0	99
97	New setup for in situ x-ray photoelectron spectroscopy from ultrahigh vacuum to 1mbar. Review of Scientific Instruments, 2005, 76, 014102.	1.3	98
98	Ternary nickel–tungsten–copper alloy rivals platinum for catalyzing alkaline hydrogen oxidation. Nature Communications, 2021, 12, 2686.	12.8	98
99	Bi2WO6 hollow microspheres with high specific surface area and oxygen vacancies for efficient photocatalysis N2 fixation. Chemical Engineering Journal, 2021, 414, 128827.	12.7	97
100	Production of Nitrogen-Doped Graphene by Low-Energy Nitrogen Implantation. Journal of Physical Chemistry C, 2012, 116, 5062-5066.	3.1	96
101	Quasi Pd1Ni single-atom surface alloy catalyst enables hydrogenation of nitriles to secondary amines. Nature Communications, 2019, 10, 4998.	12.8	90
102	Single Ni sites distributed on N-doped carbon for selective hydrogenation of acetylene. Chemical Communications, 2017, 53, 11568-11571.	4.1	88
103	Efficient infrared light induced CO2 reduction with nearly 100% CO selectivity enabled by metallic CoN porous atomic layers. Nano Energy, 2020, 69, 104421.	16.0	88
104	Regulating the Interfacial Electronic Coupling of Fe ₂ N via Orbital Steering for Hydrogen Evolution Catalysis. Advanced Materials, 2020, 32, e1904346.	21.0	86
105	An efficient room temperature core–shell AgPd@MOF catalyst for hydrogen production from formic acid. Nanoscale, 2015, 7, 8321-8325.	5.6	85
106	Energy-level modulation of non-fullerene acceptors to achieve high-efficiency polymer solar cells at a diminished energy offset. Journal of Materials Chemistry A, 2017, 5, 9649-9654.	10.3	83
107	On-Surface Pseudo-High-Dilution Synthesis of Macrocycles: Principle and Mechanism. ACS Nano, 2017, 11, 5070-5079.	14.6	83
108	Growth, Structure, and Stability of Ag on CeO ₂ (111): Synchrotron Radiation Photoemission Studies. Journal of Physical Chemistry C, 2011, 115, 6715-6725.	3.1	78

#	Article	IF	CITATIONS
109	Carbon dots decorated ultrathin CdS nanosheets enabling in-situ anchored Pt single atoms: A highly efficient solar-driven photocatalyst for hydrogen evolution. Applied Catalysis B: Environmental, 2019, 259, 118036.	20.2	77
110	In situ high-resolution XPS studies on adsorption of NO on Pt(111). Surface Science, 2003, 529, 384-396.	1.9	76
111	Confined Synthesis of Organometallic Chains and Macrocycles by Cu–O Surface Templating. ACS Nano, 2016, 10, 3747-3754.	14.6	73
112	Confined on-surface organic synthesis: Strategies and mechanisms. Surface Science Reports, 2019, 74, 97-140.	7.2	71
113	Selective CO ₂ Photoreduction into C ₂ Product Enabled by Charge-Polarized Metal Pair Sites. Nano Letters, 2021, 21, 2324-2331.	9.1	71
114	Surfactant-assisted synthesis of lanthanide metal-organic framework nanorods and their fluorescence sensing of nitroaromatic explosives. Materials Letters, 2011, 65, 1385-1387.	2.6	68
115	Thiophene Fused Azacoronenes: Regioselective Synthesis, Self-Organization, Charge Transport and Its Incorporation in Conjugated Polymers. Chemistry of Materials, 2014, 26, 3920-3927.	6.7	68
116	Kinetic Strategies for the Formation of Graphyne Nanowires via Sonogashira Coupling on Ag(111). Journal of the American Chemical Society, 2018, 140, 13421-13428.	13.7	68
117	One-Step Construction of a Hollow Au@Bimetal–Organic Framework Core–Shell Catalytic Nanoreactor for Selective Alcohol Oxidation Reaction. ACS Applied Materials & Interfaces, 2021, 13, 12463-12471.	8.0	68
118	Activated adsorption of methane on Pt(1 1 1) —anin situXPS study. New Journal of Physics, 2005, 7, 107-107.	2.9	67
119	A Stable and Efficient Cathode for Fluorineâ€Containing Protonâ€Conducting Solid Oxide Fuel Cells. ChemSusChem, 2018, 11, 3423-3430.	6.8	67
120	On-surface synthesis and characterization of individual polyacetylene chains. Nature Chemistry, 2019, 11, 924-930.	13.6	67
121	Covalent, Organometallic, and Halogen-Bonded Nanomeshes from Tetrabromo-Terphenyl by Surface-Assisted Synthesis on Cu(111). Journal of Physical Chemistry C, 2014, 118, 13018-13025.	3.1	66
122	MOF-Derived Ultrathin Cobalt Phosphide Nanosheets as Efficient Bifunctional Hydrogen Evolution Reaction Electrocatalysts. Nanomaterials, 2018, 8, 89.	4.1	66
123	Towards full-spectrum photocatalysis: Achieving a Z-scheme between Ag2S and TiO2 by engineering energy band alignment with interfacial Ag. Nano Research, 2015, 8, 3621-3629.	10.4	65
124	Polymorphic cobalt diselenide as extremely stable electrocatalyst in acidic media via a phase-mixing strategy. Nature Communications, 2019, 10, 5338.	12.8	65
125	Metal Charge Transfer Doped Carbon Dots with Reversibly Switchable, Ultra-High Quantum Yield Photoluminescence. ACS Applied Nano Materials, 2018, 1, 1886-1893.	5.0	64
126	Mesoporous Pd@Ru Core–Shell Nanorods for Hydrogen Evolution Reaction in Alkaline Solution. ACS Applied Materials & Interfaces, 2018, 10, 34147-34152.	8.0	64

#	Article	IF	CITATIONS
127	Nobleâ€Metalâ€Free Janusâ€like Structures by Cation Exchange for Zâ€6cheme Photocatalytic Water Splitting under Broadband Light Irradiation. Angewandte Chemie, 2017, 129, 4270-4274.	2.0	62
128	Scaledâ€Up Synthesis of Amorphous NiFeMo Oxides and Their Rapid Surface Reconstruction for Superior Oxygen Evolution Catalysis. Angewandte Chemie, 2019, 131, 15919-15924.	2.0	62
129	Strongly Coupled Cobalt Diselenide Monolayers for Selective Electrocatalytic Oxygen Reduction to H ₂ O ₂ under Acidic Conditions. Angewandte Chemie - International Edition, 2021, 60, 26922-26931.	13.8	61
130	From covalent triazine-based frameworks to N-doped porous carbon/reduced graphene oxide nanosheets: efficient electrocatalysts for oxygen reduction. Journal of Materials Chemistry A, 2017, 5, 23170-23178.	10.3	60
131	Efficient Photooxidation of Methane to Liquid Oxygenates over ZnO Nanosheets at Atmospheric Pressure and Near Room Temperature. Nano Letters, 2021, 21, 4122-4128.	9.1	60
132	A Critical Review on Black Phosphorusâ€Based Photocatalytic CO ₂ Reduction Application. Small, 2021, 17, e2102155.	10.0	60
133	Room-Temperature Photooxidation of CH ₄ to CH ₃ OH with Nearly 100% Selectivity over Hetero-ZnO/Fe ₂ O ₃ Porous Nanosheets. Journal of the American Chemical Society, 2022, 144, 12357-12366.	13.7	59
134	Highly Stable Grapheneâ€Based Multilayer Films Immobilized via Covalent Bonds and Their Applications in Organic Fieldâ€Effect Transistors. Advanced Functional Materials, 2013, 23, 2422-2435.	14.9	56
135	In Situ Topotactic Transformation of an Interstitial Alloy for CO Electroreduction. Advanced Materials, 2020, 32, e2002382.	21.0	56
136	Hollow CuS Nanoboxes as Liâ€Free Cathode for Highâ€Rate and Longâ€Life Lithium Metal Batteries. Advanced Energy Materials, 2020, 10, 1903401.	19.5	56
137	Conversion reaction of vanadium sulfide electrode in the lithium-ion cell: Reversible or not reversible?. Nano Energy, 2018, 51, 391-399.	16.0	55
138	Selective on-surface covalent coupling based on metal-organic coordination template. Nature Communications, 2019, 10, 70.	12.8	55
139	Kinetics of the CO oxidation reaction on Pt(111) studied by in situ high-resolution x-ray photoelectron spectroscopy. Journal of Chemical Physics, 2004, 120, 7113-7122.	3.0	54
140	Surface-Limited Superconducting Phase Transition on 1 <i>T</i> -TaS ₂ . ACS Nano, 2018, 12, 12619-12628.	14.6	54
141	Porosity-induced emission: exploring color-controllable fluorescence of porous organic polymers and their chemical sensing applications. Journal of Materials Chemistry C, 2015, 3, 6876-6881.	5.5	53
142	Hierarchical Dehydrogenation Reactions on a Copper Surface. Journal of the American Chemical Society, 2018, 140, 6076-6082.	13.7	53
143	Unveiling the Active Site of Metal-Free Nitrogen-doped Carbon for Electrocatalytic Carbon Dioxide Reduction. Cell Reports Physical Science, 2020, 1, 100145.	5.6	53
144	Organic additive-free synthesis of mesocrystalline hematite nanoplates via two-dimensional oriented attachment. CrystEngComm, 2014, 16, 1553-1559.	2.6	52

#	Article	IF	CITATIONS
145	Synthesis of Monolayer Blue Phosphorus Enabled by Silicon Intercalation. ACS Nano, 2020, 14, 3687-3695.	14.6	52
146	Steering Unit Cell Dipole and Internal Electric Field by Highly Dispersed Er atoms Embedded into NiO for Efficient CO ₂ Photoreduction. Advanced Functional Materials, 2022, 32, .	14.9	52
147	Vibrationally resolved in situ XPS study of activated adsorption of methane on Pt(111). Chemical Physics Letters, 2004, 390, 208-213.	2.6	51
148	A site-selective in situ study of CO adsorption and desorption on Pt(355). Journal of Chemical Physics, 2006, 124, 074712.	3.0	51
149	High adsorption capacity and the key role of carbonate groups for heavy metal ion removal by basic aluminum carbonate porous nanospheres. Journal of Materials Chemistry, 2012, 22, 19898.	6.7	51
150	Promoting desulfurization capacity and separation efficiency simultaneously by the novel magnetic Fe ₃ O ₄ @PAA@MOF-199. RSC Advances, 2014, 4, 41902-41909.	3.6	50
151	Facile synthesis of highly luminescent nanowires of a terbium-based metal–organic framework by an ultrasonic-assisted method and their application as a luminescent probe for selective sensing of organoamines. Inorganic Chemistry Communication, 2012, 17, 147-150.	3.9	49
152	Metal–organic gel templated synthesis of magnetic porous carbon for highly efficient removal of organic dyes. Dalton Transactions, 2016, 45, 4541-4547.	3.3	49
153	Surface Adatom Mediated Structural Transformation in Bromoarene Monolayers: Precursor Phases in Surface Ullmann Reaction. ACS Nano, 2018, 12, 2267-2274.	14.6	49
154	Electrochemical activity of 1T′ structured rhenium selenide nanosheets <i>via</i> electronic structural modulation from selenium-vacancy generation. Journal of Materials Chemistry A, 2018, 6, 22526-22533.	10.3	49
155	Anchoring Pt Single Atoms on Te Nanowires for Plasmonâ€Enhanced Dehydrogenation of Formic Acid at Room Temperature. Advanced Science, 2019, 6, 1900006.	11.2	49
156	Nitrogen doped FeS2 nanoparticles for efficient and stable hydrogen evolution reaction. Journal of Energy Chemistry, 2021, 56, 283-289.	12.9	49
157	Surface Science Studies on the Zirconia-Based Model Catalysts. Topics in Catalysis, 2013, 56, 1525-1541.	2.8	48
158	Near-surface dilution of trace Pd atoms to facilitate Pd-H bond cleavage for giant enhancement of electrocatalytic hydrogen evolution. Nano Energy, 2017, 34, 306-312.	16.0	48
159	Selective CO ₂ Photoreduction to CH ₄ via Pd ^{<i>δ</i>+} â€Assisted Hydrodeoxygenation over CeO ₂ Nanosheets. Angewandte Chemie - International Edition, 2022, 61, .	13.8	48
160	High-performance lithium/sulfur cells with a bi-functionally immobilized sulfur cathode. Nano Energy, 2014, 9, 408-416.	16.0	47
161	Core–shell nanoporous AuCu ₃ @Au monolithic electrode for efficient electrochemical CO ₂ reduction. Journal of Materials Chemistry A, 2020, 8, 3344-3350.	10.3	46
162	Calcium Adsorption on MgO(100):  Energetics, Structure, and Role of Defects. Journal of the American Chemical Society, 2008, 130, 2314-2322.	13.7	45

#	Article	IF	CITATIONS
163	Three-dimensional porous Fe0.1V2O5.15 thin film as a cathode material for lithium ion batteries. Electrochimica Acta, 2012, 64, 81-86.	5.2	45
164	Modulate Organicâ€Metal Oxide Heterojunction via [1,6] Azafulleroid for Highly Efficient Organic Solar Cells. Advanced Materials, 2016, 28, 7269-7275.	21.0	45
165	Organic dye doped graphitic carbon nitride with a tailored electronic structure for enhanced photocatalytic hydrogen production. Catalysis Science and Technology, 2019, 9, 502-508.	4.1	45
166	An Efficient Turingâ€Type Ag ₂ Seâ€CoSe ₂ Multiâ€Interfacial Oxygenâ€Evolving Electrocatalyst**. Angewandte Chemie - International Edition, 2021, 60, 6553-6560.	13.8	45
167	Coordination reaction between tetraphenylporphyrin and nickel on a TiO ₂ (110) surface. Chemical Communications, 2014, 50, 8291-8294.	4.1	44
168	Coadsorption of D2O and CO on Pt(111) Studied by in Situ High-Resolution X-ray Photoelectron Spectroscopy. Langmuir, 2004, 20, 1819-1826.	3.5	43
169	Rechargeable Aluminium–Sulfur Battery with Improved Electrochemical Performance by Cobaltâ€Containing Electrocatalyst. Angewandte Chemie - International Edition, 2020, 59, 22963-22967.	13.8	43
170	Highly Selective Synthesis of <i>cis</i> â€Enediynes on a Ag(111) Surface. Angewandte Chemie - International Edition, 2017, 56, 4762-4766.	13.8	42
171	MOC-derived porous FeCo/C nanocomposites as a potential platform for enhanced catalytic activity and lithium-ion batteries performance. Journal of Colloid and Interface Science, 2018, 522, 283-290.	9.4	42
172	Nickel Doping in Atomically Thin Tin Disulfide Nanosheets Enables Highly Efficient CO ₂ Reduction. Angewandte Chemie, 2018, 130, 11120-11124.	2.0	42
173	Plastics-to-syngas photocatalysed by Co–Ga2O3 nanosheets. National Science Review, 2022, 9, .	9.5	42
174	Formation of the Calcium/Poly(3-Hexylthiophene) Interface: Structure and Energetics. Journal of the American Chemical Society, 2009, 131, 13498-13507.	13.7	41
175	Visibleâ€Lightâ€Driven Overall Water Splitting Boosted by Tetrahedrally Coordinated Blende Cobalt(II) Oxide Atomic Layers. Angewandte Chemie - International Edition, 2019, 58, 3032-3036.	13.8	41
176	Ag Nanoparticles on Reducible CeO ₂ (111) Thin Films: Effect of Thickness and Stoichiometry of Ceria. Journal of Physical Chemistry C, 2015, 119, 3579-3588.	3.1	40
177	Intermediate States Directed Chiral Transfer on a Silver Surface. Journal of the American Chemical Society, 2019, 141, 168-174.	13.7	40
178	Electrochemical conversion of bulk platinum into platinum single-atom sites for the hydrogen evolution reaction. Journal of Materials Chemistry A, 2020, 8, 10755-10760.	10.3	40
179	Fabrication of oxygen-doped MoSe2 hierarchical nanosheets for highly sensitive and selective detection of trace trimethylamine at room temperature in air. Nano Research, 2020, 13, 1704-1712.	10.4	39
180	Calibration strategy of the JUNO experiment. Journal of High Energy Physics, 2021, 2021, 1.	4.7	39

#	Article	IF	CITATIONS
181	General Synthesis of Tube-like Nanostructured Perovskite Oxides with Tunable Transition Metal–Oxygen Covalency for Efficient Water Electrooxidation in Neutral Media. Journal of the American Chemical Society, 2022, 144, 13163-13173.	13.7	39
182	Tribromobenzene on Cu(111): Temperature-dependent formation of halogen-bonded, organometallic, and covalent nanostructures. Journal of Chemical Physics, 2015, 142, 101906.	3.0	38
183	Chiral Kagome Lattices from Onâ€Surface Synthesized Molecules. ChemPhysChem, 2017, 18, 3329-3333.	2.1	38
184	Unravelling the Mechanism of Glaser Coupling Reaction on Ag(111) and Cu(111) Surfaces: a Case for Halogen Substituted Terminal Alkyne. Journal of Physical Chemistry C, 2018, 122, 14537-14545.	3.1	38
185	Water Additive Enhanced Solution Processing of Alloy Sb ₂ (S _{1â^'<i>x</i>} Se _{<i>x</i>}) ₃ â€Based Solar Cells. Solar Rrl, 2020, 4, 1900582.	5.8	38
186	Interplay between Interfacial Structures and Device Performance in Organic Solar Cells: A Case Study with the Low Work Function Metal, Calcium. ACS Applied Materials & amp; Interfaces, 2016, 8, 2125-2131.	8.0	37
187	Feasible Modification of PEDOT:PSS by Poly(4-styrenesulfonic acid): A Universal Method to Double the Efficiencies for Solution-Processed Organic Light-Emitting Devices. ACS Applied Materials & Interfaces, 2019, 11, 29105-29112.	8.0	37
188	Efficient photoelectrochemical CO2 conversion for selective acetic acid production. Science Bulletin, 2021, 66, 1296-1304.	9.0	37
189	Dynamic Atom Clusters on AuCu Nanoparticle Surface during CO Oxidation. Journal of the American Chemical Society, 2020, 142, 4022-4027.	13.7	36
190	TiN nanocrystal anchored on N-doped graphene as effective sulfur hosts for high-performance lithium-sulfur batteries. Journal of Energy Chemistry, 2021, 54, 16-22.	12.9	35
191	Over 1 GW/cm ₂ Vertical Ga ₂ O ₃ Schottky Barrier Diodes Without Edge Termination. IEEE Electron Device Letters, 2022, 43, 264-267.	3.9	34
192	Single palladium atoms stabilized by \hat{l}^2 -FeOOH nanorod with superior performance for selective hydrogenation of cinnamaldehyde. Nano Research, 2022, 15, 3114-3121.	10.4	34
193	Ferroelectric control of single-molecule magnetism in 2D limit. Science Bulletin, 2020, 65, 1252-1259.	9.0	33
194	Double-site defect passivation of perovskite film via fullerene additive engineering toward highly efficient and stable bulk heterojunction solar cells. Nano Today, 2021, 39, 101164.	11.9	33
195	Hydroxyl Group Rich C ₆₀ Fullerenol: An Excellent Hydrogen Bond Catalyst with Superb Activity, Selectivity, and Stability. ACS Catalysis, 2011, 1, 1158-1161.	11.2	32
196	Electronic structure study of ordering and interfacial interaction in graphene/Cu composites. Carbon, 2012, 50, 5316-5322.	10.3	32
197	X-ray Absorption Spectroscopy Characterization of a Li/S Cell. Nanomaterials, 2016, 6, 14.	4.1	32
198	The role of the substrate structure in the on-surface synthesis of organometallic and covalent oligophenylene chains. Physical Chemistry Chemical Physics, 2016, 18, 20627-20634.	2.8	32

#	Article	IF	CITATIONS
199	Dualâ€Metal Sites Boosting Polarization of Nitrogen Molecules for Efficient Nitrogen Photofixation. Advanced Science, 2021, 8, 2100302.	11.2	32
200	Cracked-earth-like titanium carbide MXene membranes with abundant hydroxyl groups for oil-in-water emulsion separation. Journal of Colloid and Interface Science, 2022, 607, 378-388.	9.4	32
201	Ca Carboxylate Formation at the Calcium/Poly(methyl methacrylate) Interface. Journal of Physical Chemistry C, 2012, 116, 20465-20471.	3.1	31
202	Metaln+-Metalδ+ pair sites steer C-C coupling for selective CO2 photoreduction to C2 hydrocarbons. Nano Research, 2022, 15, 1882-1891.	10.4	31
203	Hungry Porphyrins: Protonation and Selfâ€Metalation of Tetraphenylporphyrin on TiO ₂ (110) ―1 × 1. ChemistrySelect, 2016, 1, 6103-6105.	1.5	30
204	Interface Formation between Calcium and Electron-Irradiated Poly(3-hexylthiophene). Langmuir, 2010, 26, 9632-9639.	3.5	29
205	Chiral recognition of zinc phthalocyanine on Cu(100) surface. Applied Physics Letters, 2012, 100, 081602.	3.3	28
206	Electronic band structure of graphene from resonant soft x-ray spectroscopy: The role of core-hole effects. Physical Review B, 2012, 86, .	3.2	28
207	Temperature-induced structural evolution of Sm nanoparticles on Al2O3 thin film: An in-situ investigation using SRPES, XPS and STM. Applied Surface Science, 2018, 432, 115-120.	6.1	28
208	Enabling Visibleâ€Lightâ€Driven Selective CO ₂ Reduction by Doping Quantum Dots: Trapping Electrons and Suppressing H ₂ Evolution. Angewandte Chemie, 2018, 130, 16685-16689.	2.0	28
209	Supramolecular Tessellations at Surfaces by Vertex Design. ACS Nano, 2019, 13, 10603-10611.	14.6	28
210	Reaction selectivity of homochiral versus heterochiral intermolecular reactions of prochiral terminal alkynes on surfaces. Nature Communications, 2019, 10, 4122.	12.8	27
211	The band offset at CdS/Cu2ZnSnS4 heterojunction interface. Electronic Materials Letters, 2012, 8, 365-367.	2.2	26
212	Interaction of Au with Thin ZrO ₂ Films: Influence of ZrO ₂ Morphology on the Adsorption and Thermal Stability of Au Nanoparticles. Langmuir, 2012, 28, 6045-6051.	3.5	26
213	Electrostatic spray deposition of porous Fe2V4O13 films as electrodes for Li-ion batteries. Journal of Alloys and Compounds, 2012, 520, 77-82.	5.5	26
214	Surface passivation of black phosphorus via van der Waals stacked PTCDA. Applied Surface Science, 2019, 496, 143688.	6.1	26
215	Ethene adsorption and dehydrogenation on clean and oxygen precovered Ni(111) studied by high resolution x-ray photoelectron spectroscopy. Journal of Chemical Physics, 2010, 133, 014706.	3.0	25
216	On-Surface Synthesis of Armchair-Edged Graphene Nanoribbons with Zigzag Topology. Journal of Physical Chemistry C, 2020, 124, 5248-5256.	3.1	25

#	Article	IF	CITATIONS
217	Carbon-coated Fe2O3 hollow sea urchin nanostructures as high-performance anode materials for lithium-ion battery. Science China Materials, 2021, 64, 307-317.	6.3	25
218	Direct Formation of C–C Double-Bonded Structural Motifs by On-Surface Dehalogenative Homocoupling of <i>gem</i> -Dibromomethyl Molecules. ACS Nano, 2018, 12, 7959-7966.	14.6	24
219	Comprehensive electronic structure characterization of pristine and nitrogen/phosphorus doped carbon nanocages. Carbon, 2016, 103, 480-487.	10.3	23
220	Highly Degenerate Ground States in a Frustrated Antiferromagnetic Kagome Lattice in a Two-Dimensional Metal–Organic Framework. Journal of Physical Chemistry Letters, 2021, 12, 3733-3739.	4.6	23
221	Boosting photoelectrochemical efficiency by near-infrared-active lattice-matched morphological heterojunctions. Nature Communications, 2021, 12, 4296.	12.8	23
222	Synergizing Surface Hydride Species and Ru Clusters on Sm ₂ O ₃ for Efficient Ammonia Synthesis. ACS Catalysis, 2022, 12, 2178-2190.	11.2	23
223	Role of oxygen incorporation in electronic properties of rubrene films. Applied Physics Letters, 2010, 97, 032106.	3.3	22
224	Interaction of Zr with CeO ₂ (111) Thin Film and Its Influence on Supported Ag Nanoparticles. Journal of Physical Chemistry C, 2015, 119, 18257-18266.	3.1	22
225	Tracking the Local Effect of Fluorine Self-Doping in Anodic TiO ₂ Nanotubes. Journal of Physical Chemistry C, 2016, 120, 4623-4628.	3.1	22
226	Enhancing electrochemical nitrogen reduction with Ru nanowires <i>via</i> the atomic decoration of Pt. Journal of Materials Chemistry A, 2020, 8, 25142-25147.	10.3	22
227	Tuning the Interaction between Ruthenium Single Atoms and the Second Coordination Sphere for Efficient Nitrogen Photofixation. Advanced Functional Materials, 2022, 32, .	14.9	22
228	Adsorption Energy, Growth Mode, and Sticking Probability of Ca on Poly(methyl methacrylate) Surfaces with and without Electron Damage. Journal of the American Chemical Society, 2007, 129, 6432-6441.	13.7	21
229	Low energy Ar-ion bombardment effects on the CeO2 surface. Applied Surface Science, 2012, 258, 2057-2061.	6.1	21
230	Simultaneous reduction and N-doping of graphene oxides by low-energy N2+ ion sputtering. Carbon, 2013, 62, 365-373.	10.3	21
231	Enhanced O2 reduction on atomically thin Pt-based nanoshells by integrating surface facet, interfacial electronic, and substrate stabilization effects. Nano Research, 2018, 11, 3313-3326.	10.4	21
232	Interfacial electronic interaction of atomically dispersed IrClx on ultrathin Co(OH)2/CNTs for efficient electrocatalytic water oxidation. Applied Catalysis B: Environmental, 2020, 279, 119398.	20.2	21
233	Hydrodeoxygenation of lignin-derived phenolics over facile prepared bimetallic RuCoNx/NC. Fuel, 2022, 308, 121979.	6.4	21
234	Heats of adsorption of Pb on pristine and electron-irradiated poly(methyl methacrylate) by microcalorimetry. Surface Science, 2005, 598, 22-34.	1.9	20

#	Article	IF	CITATIONS
235	Lithium adsorption on MgO(100) and its defects: Charge transfer, structure, and energetics. Physical Review B, 2009, 80, .	3.2	20
236	Metalation of tetraphenylporphyrin with nickel on a TiO2(110)-1 × 2 surface. Nanoscale, 2016, 8, 1123-1132.	5.6	20
237	Low-Temperature Dissociation of CO ₂ on a Ni/CeO ₂ (111)/Ru(0001) Model Catalyst. Journal of Physical Chemistry C, 2016, 120, 5980-5987.	3.1	20
238	Interaction between Cu Nanoparticles and CeO ₂ (111) Film Surfaces. Journal of Physical Chemistry C, 2019, 123, 23563-23571.	3.1	20
239	Chemisorption-Induced Formation of Biphenylene Dimer on Ag(111). Journal of the American Chemical Society, 2022, 144, 723-732.	13.7	20
240	The adsorption of NO on an oxygen pre-covered Pt(111) surface: in situ high-resolution XPS combined with molecular beam studies. Surface Science, 2003, 547, 410-420.	1.9	19
241	Pyroelectric heat detector for measuring adsorption energies on thicker single crystals. Sensors and Actuators B: Chemical, 2005, 107, 454-460.	7.8	19
242	Iron Resonant Photoemission Spectroscopy on Anodized Hematite Points to Electron Hole Doping during Anodization. ChemPhysChem, 2012, 13, 2937-2944.	2.1	19
243	Interaction of Mn with reducible CeO2(111) thin films. Applied Surface Science, 2013, 283, 1-5.	6.1	19
244	Top-down fabrication of hematite mesocrystals with tunable morphologies. CrystEngComm, 2013, 15, 6284.	2.6	19
245	Between photocatalysis and photosynthesis: Synchrotron spectroscopy methods on molecules and materials for solar hydrogen generation. Journal of Electron Spectroscopy and Related Phenomena, 2013, 190, 93-105.	1.7	18
246	Structural and Optical Interplay of Palladium-Modified TiO ₂ Nanoheterostructure. Journal of Physical Chemistry C, 2015, 119, 2222-2230.	3.1	18
247	Surface Modification on Pd Nanostructures for Selective Styrene Oxidation with Molecular Oxygen. ChemNanoMat, 2018, 4, 467-471.	2.8	18
248	MIL-100(Al) Gels as an Excellent Platform Loaded with Doxorubicin Hydrochloride for pH-Triggered Drug Release and Anticancer Effect. Nanomaterials, 2018, 8, 446.	4.1	18
249	In Situ Investigations of Al/Perovskite Interfacial Structures. ACS Applied Materials & Interfaces, 2020, 12, 28861-28868.	8.0	18
250	<i>In situ</i> investigation of interfacial properties of Sb2Se3 heterojunctions. Applied Physics Letters, 2020, 116, .	3.3	18
251	Intercalation of Li at the Graphene/Cu Interface. Journal of Physical Chemistry C, 2013, 117, 9259-9265.	3.1	17
252	Visibleâ€Lightâ€Driven Overall Water Splitting Boosted by Tetrahedrally Coordinated Blende Cobalt(II) Oxide Atomic Layers. Angewandte Chemie, 2019, 131, 3064-3068.	2.0	17

#	Article	IF	CITATIONS
253	Photocatalytic Conversion of Waste Plastics into C ₂ Fuels under Simulated Natural Environment Conditions. Angewandte Chemie, 2020, 132, 15627-15631.	2.0	17
254	Low-temperature phases of Xe on Pd(111). Physical Review B, 2003, 68, .	3.2	16
255	Growth, Structure, and Stability of Au on Ordered ZrO ₂ (111) Thin Films. Journal of Physical Chemistry C, 2011, 115, 10744-10751.	3.1	16
256	Electronic structures and chemical reactions at the interface between Li and regioregular poly (3-hexylthiophene). Organic Electronics, 2012, 13, 1060-1067.	2.6	16
257	Stability and protection of nanowire devices in air. Nano Research, 2018, 11, 3353-3361.	10.4	16
258	Oxygen modified CoP2 supported palladium nanoparticles as highly efficient catalyst for hydrolysis of ammonia borane. Nano Research, 2022, 15, 3034-3041.	10.4	16
259	Modulation of BiOBr-based photocatalysts for energy and environmental application: A critical review. Journal of Environmental Chemical Engineering, 2022, 10, 107226.	6.7	16
260	Selective synthesis of Kagome nanoporous graphene on Ag(111) <i>via</i> an organometallic template. Nanoscale, 2022, 14, 6239-6247.	5.6	16
261	Surface Engineering on Commercial Cu Foil for Steering C ₂ H ₄ /CH ₄ Ratio in CO ₂ Electroreduction. Nano Letters, 2022, 22, 2988-2994.	9.1	16
262	Single-Atom Manganese Anchored on Carbon Dots for Promoting Mitochondrial Targeting and Photodynamic Effect in Cancer Treatment. ACS Applied Nano Materials, 2022, 5, 6679-6690.	5.0	16
263	Spontaneous Bulk-Surface Charge Separation of TiO ₂ -{001} Nanocrystals Leads to High Activity in Photocatalytic Methane Combustion. ACS Catalysis, 2022, 12, 6457-6463.	11.2	16
264	Epitaxial growth of ultrathin ZrO2(111) films on Pt(111). Science Bulletin, 2011, 56, 502-507.	1.7	15
265	Competitive Adsorption between a Polymer and Its Monomeric Analog Enables Precise Modulation of Nanowire Synthesis. CheM, 2018, 4, 2451-2462.	11.7	15
266	Proton-free electron-trapping feature of titanium dioxide nanoparticles without the characteristic blue color. Communications Chemistry, 2019, 2, .	4.5	15
267	Topology Selectivity in On-Surface Dehydrogenative Coupling Reaction: Dendritic Structure <i>versus</i> Porous Graphene Nanoribbon. ACS Nano, 2021, 15, 4617-4626.	14.6	15
268	The design and sensitivity of JUNO's scintillator radiopurity pre-detector OSIRIS. European Physical Journal C, 2021, 81, 1.	3.9	15
269	Atomically Defined Undercoordinated Copper Active Sites over Nitrogenâ€Doped Carbon for Aerobic Oxidation of Alcohols. Small, 2022, 18, e2106614.	10.0	15
270	Growth and electronic structure of Sm on thin Al2O3/Ni3Al(111) films. Journal of Chemical Physics, 2012, 136, 154705.	3.0	14

#	Article	IF	CITATIONS
271	Decarboxylation of Fatty Acids on Anisotropic Au(110) Surfaces. Journal of Physical Chemistry C, 2018, 122, 9075-9080.	3.1	14
272	Understanding the electrochemical reaction mechanism of VS ₂ nanosheets in lithium-ion cells by multiple <i>in situ</i> and <i>ex situ</i> x-ray spectroscopy. Journal Physics D: Applied Physics, 2018, 51, 494001.	2.8	14
273	Noncovalent phosphorylation of graphene oxide with improved hole transport in high-efficiency polymer solar cells. Nanoscale, 2018, 10, 14840-14846.	5.6	14
274	Surface Modification on Pdâ€īiO 2 Hybrid Nanostructures towards Highly Efficient H 2 Production from Catalytic Formic Acid Decomposition. Chemistry - A European Journal, 2018, 24, 18398-18402.	3.3	14
275	Nickel Adatoms Induced Tautomeric Dehydrogenation of Thymine Molecules on Au(111). ACS Nano, 2018, 12, 9033-9039.	14.6	14
276	<i>In situ</i> investigations of interfacial degradation and ion migration at CH3NH3PbI3 perovskite/Ag interface. Chinese Journal of Chemical Physics, 2019, 32, 299-305.	1.3	14
277	On-Surface Synthesis of Chiral π-Conjugate Porphyrin Tapes by Substrate-Regulated Dehydrogenative Coupling. Journal of Physical Chemistry C, 2019, 123, 23007-23013.	3.1	14
278	In2O3 Nanocrystals for CO2 Fixation: Atomic-Level Insight into the Role of Grain Boundaries. IScience, 2019, 16, 390-398.	4.1	14
279	Ultrastable and Efficient Visibleâ€lightâ€driven CO ₂ Reduction Triggered by Regenerative Oxygenâ€Vacancies in Bi ₂ O ₂ CO ₃ Nanosheets. Angewandte Chemie, 2021, 133, 13959-13965.	2.0	14
280	Electronic structure of PCBM. Chinese Physics B, 2012, 21, 017102.	1.4	13
281	Targeted design and synthesis of a highly selective Mo-based catalyst for the synthesis of higher alcohols. RSC Advances, 2016, 6, 38741-38745.	3.6	13
282	X-ray Absorption Spectroscopic Characterization of the Synthesis Process: Revealing the Interactions in Cetyltrimethylammonium Bromide-Modified Sulfur–Graphene Oxide Nanocomposites. Journal of Physical Chemistry C, 2016, 120, 10111-10117.	3.1	13
283	Highly Selective Synthesis of <i>cis</i> â€Enediynes on a Ag(111) Surface. Angewandte Chemie, 2017, 129, 4840-4844.	2.0	13
284	Catalytic Performance of Novel Hierarchical Porous Flower-Like NiCo2O4 Supported Pd in Lean Methane Oxidation. Catalysis Letters, 2018, 148, 2799-2811.	2.6	13
285	Construction of molecular regular tessellations on a Cu(111) surface. Chemical Communications, 2018, 54, 7010-7013.	4.1	13
286	Band Structure Engineering toward Low-Onset-Potential Photoelectrochemical Hydrogen Production. , 2020, 2, 1555-1560.		13
287	Alkali metal storage mechanism in organic semiconductor of perylene-3,4,9,10-tetracarboxylicdianhydride. Applied Surface Science, 2020, 524, 146396.	6.1	13
288	The construction of NiFeS _x /g-C ₃ N ₄ composites with high photocatalytic activity towards the degradation of refractory pollutants. Dalton Transactions, 2021, 50, 2436-2447.	3.3	13

#	Article	IF	CITATIONS
289	Radioactivity control strategy for the JUNO detector. Journal of High Energy Physics, 2021, 2021, 1.	4.7	13
290	Preparation and adsorption properties of Mo2N model catalyst. Applied Surface Science, 2000, 161, 86-93.	6.1	12
291	Dechlorinated Ullmann Coupling Reaction of Aryl Chlorides on Ag(111): A Combined STM and XPS Study. ChemPhysChem, 2019, 20, 2367-2375.	2.1	12
292	Kinetic Control over Morphology of Nanoporous Graphene on Surface. ChemPhysChem, 2019, 20, 2327-2332.	2.1	12
293	Probing reaction pathways for H2O-mediated HCHO photooxidation at room temperature. Nano Research, 2021, 14, 1471-1478.	10.4	12
294	Synergistic catalysis of cluster and atomic copper induced by copper-silica interface in transfer-hydrogenation. Nano Research, 2021, 14, 4601-4609.	10.4	12
295	Atmospheric CO2 capture and photofixation to near-unity CO by Ti3+-Vo-Ti3+ sites confined in TiO2 ultrathin layers. Science China Chemistry, 2021, 64, 953-958.	8.2	12
296	Synchrotron-Radiation Photoemission Study of Growth and Stability of Au Clusters on Rutile TiO2(110)-1 1. Chinese Journal of Chemical Physics, 2009, 22, 339-345.	1.3	11
297	Electronic structure and chemical reaction of Ca deposition on regioregular poly(3-hexylthiophene) surfaces. Science Bulletin, 2009, 54, 1978-1982.	9.0	11
298	Study of Au/Hg3In2Te6interface by synchrotron radiation photoemission spectroscopy. Journal of Applied Physics, 2013, 114, 083719.	2.5	11
299	Interaction of Zr with oxidized and partially reduced ceria thin films. Surface Science, 2016, 653, 205-210.	1.9	11
300	An in-situ spectroscopy investigation of alkali metal interaction mechanism with the imide functional group. Nano Research, 2020, 13, 3224-3229.	10.4	11
301	Efficient Infraredâ€Lightâ€Driven CO ₂ Reduction Over Ultrathin Metallic Niâ€doped CoS ₂ Nanosheets. Angewandte Chemie, 2021, 133, 8787-8791.	2.0	11
302	Structure Sensitivity of Auâ€TiO 2 Strong Metal–Support Interactions. Angewandte Chemie, 2021, 133, 12181-12188.	2.0	11
303	JUNO sensitivity to low energy atmospheric neutrino spectra. European Physical Journal C, 2021, 81, 1.	3.9	11
304	Photoconverting polyethylene terephthalate into exclusive carbon dioxide by heterostructured NiO/Fe2O3 nanosheets under mild conditions. Science China Materials, 2022, 65, 985-991.	6.3	11
305	The study on the work function of CdZnTe with different surface states by synchrotron radiation photoemission spectroscopy. Journal of Applied Physics, 2009, 106, 053714.	2.5	10
306	Exploring the role of samarium in the modification of rhodium catalysts through surface science approach. Surface Science, 2009, 603, 1802-1811.	1.9	10

#	Article	IF	CITATIONS
307	Band alignment determination of ZnO/PbSe heterostructure interfaces by synchrotron radiation photoelectron spectroscopy. Europhysics Letters, 2012, 99, 37010.	2.0	10
308	Electronic properties of Cr-N codoped rutile TiO2(110) thin films. Surface Science, 2017, 666, 84-89.	1.9	10
309	Synthesis of Quasiâ€Bilayer Subnano Metalâ€Oxide Interfacial Cluster Catalysts for Advanced Catalysis. Small, 2020, 16, e2005571.	10.0	10
310	Stepwise Synthesis of N–Ag–N and C–Ag–C Organometallic Structures on a Ag(111) Surface. Journal of Physical Chemistry C, 2020, 124, 16415-16422.	3.1	10
311	Probing surface defects of ZnO using formaldehyde. Journal of Chemical Physics, 2020, 152, 074714.	3.0	10
312	Atomic structures and electronic properties of Cr-doped ZnO() surfaces. Chinese Journal of Catalysis, 2021, 42, 971-979.	14.0	10
313	Surface-assisted fabrication of low-dimensional carbon-based nanoarchitectures. Journal of Physics Condensed Matter, 2021, 33, 343001.	1.8	10
314	Interface Dipole and Schottky Barrier Formation at Au/CdZnTe(111)A Interfaces. Journal of Physical Chemistry C, 2010, 114, 16426-16429.	3.1	9
315	Band alignment of ZnO/CdSe quantum dots heterojunction determined by ultraviolet photoelectron spectroscopy using synchrotron radiation. Applied Surface Science, 2013, 276, 258-261.	6.1	9
316	Experimental Realization of One-Dimensional Metal-Inorganic Chain: Gold–Phosphorus Chain. , 2020, 2, 873-879.		9
317	Formic acid adsorption and decomposition on clean and atomic oxygen pre-covered Cu(100) surfaces. Journal of Chemical Physics, 2020, 152, 114703.	3.0	9
318	On-surface synthesis of planar acenes <i>via</i> regioselective aryl–aryl coupling. Chemical Communications, 2020, 56, 4890-4893.	4.1	9
319	NiFe-Layered Double Hydroxides as a Novel Hole Repository Layer for Reinforced Visible-Light Photocatalytic Activity for Degradation of Refractory Pollutants. Industrial & Engineering Chemistry Research, 2021, 60, 13834-13845.	3.7	9
320	Synthesis of PdS _x -Mediated Polydymite Heteronanorods and Their Long-Range Activation for Enhanced Water Electroreduction. Research, 2019, 2019, 8078549.	5.7	9
321	Synthesis and optical properties of poly[3-(2-methoxyphenyl)thiophene] nanowires confined in porous anodic alumina membrane. Optical Materials, 2008, 30, 1861-1866.	3.6	8
322	Valence band of poly(sodium 4-styrenesulfonate) intercalated graphite oxide composites. Chemical Physics Letters, 2013, 559, 67-70.	2.6	8
323	Effect of Mn Promoter on Structure and Performance of K-Co-Mo Catalyst for Synthesis of Higher Alcohols from CO Hydrogenation. Chinese Journal of Chemical Physics, 2016, 29, 671-680.	1.3	8
324	Controlling Au–Pd Surface on Au Nanocubes for Selective Catalytic Alkyne Semihydrogenation. Particle and Particle Systems Characterization, 2018, 35, 1700377.	2.3	8

#	Article	IF	CITATIONS
325	Sm on CeO2(111): A Case for Ceria Modification via Strong Metal–Ceria Interaction. Topics in Catalysis, 2018, 61, 1227-1236.	2.8	8
326	A Dopant Replacementâ€Driven Molten Salt Method toward the Synthesis of Subâ€5â€nmâ€6ized Ultrathin Nanowires. Small, 2020, 16, 2001098.	10.0	8
327	Anti-photocorrosive photoanode with RGO/PdS as hole extraction layer. Science China Materials, 2020, 63, 1939-1947.	6.3	8
328	In Situ Investigation of the Cu/CH 3 NH 3 PbI 3 Interface in Perovskite Device. Advanced Materials Interfaces, 2021, 8, 2100120.	3.7	8
329	Natural Nanofibrous Cellulose-Derived Solid Acid Catalysts. Research, 2019, 2019, 6262719.	5.7	8
330	Quasi-Monolayer Ag ₂ Se/1T-WSe ₂ Nanosheets for Enhanced Electrocatalytic Hydrogen Evolution and Charge Storage. ACS Applied Nano Materials, 2022, 5, 6410-6421.	5.0	8
331	Generating oxygen adatoms on Au(997) by thermal decomposition of NO2. Science Bulletin, 2010, 55, 3889-3893.	1.7	7
332	Energy band alignment of PbTe/CdTe(111) interface determined by ultraviolet photoelectron spectra using synchrotron radiation. Chinese Physics B, 2010, 19, 077301.	1.4	7
333	Interaction of oxygen with samarium on Al2O3 thin film grown on Ni3Al(111). Journal of Chemical Physics, 2014, 140, 094706.	3.0	7
334	Engineering the metal–organic interface by transferring a high-quality single layer graphene on top of organic materials. Carbon, 2015, 87, 78-86.	10.3	7
335	On-Surface Ullmann Reaction for the Synthesis of Polymers and Macrocycles. Advances in Atom and Single Molecule Machines, 2018, , 83-112.	0.0	7
336	Activating P2-NaxCoO2 for efficient water oxidation catalysis via controlled chemical oxidation. Materials Today Chemistry, 2018, 10, 206-212.	3.5	7
337	Stable Active Sites on Ni 12 P 5 Surfaces for the Hydrogen Evolution Reaction. Energy Technology, 2019, 7, 1900013.	3.8	7
338	Fine-tuning of two-dimensional metal–organic nanostructures <i>via</i> alkali–pyridyl coordination. Nanoscale Advances, 2020, 2, 2170-2176.	4.6	7
339	Fundamental Insights into Surface Modification of Silicon Material toward Improved Activity and Durability in Photocatalytic Hydrogen Production: A Case Study of Pre-Lithiation. Journal of Physical Chemistry C, 2021, 125, 5542-5548.	3.1	7
340	Rational design of dumbbell-like Au-Fe3O4@Carbon yolk@shell nanospheres with superior catalytic activity. Colloids and Surfaces A: Physicochemical and Engineering Aspects, 2021, 623, 126665.	4.7	7
341	Chiral nanoporous networks featuring various chiral vertices from an achiral molecule on Ag(100). Nano Research, 2022, 15, 3753-3762.	10.4	7
342	Constructing artificial mimic-enzyme catalysts for carbon dioxide electroreduction. Science China Chemistry, 2022, 65, 106-113.	8.2	7

#	Article	IF	CITATIONS
343	Revisiting Oxygen Adsorption on Ir(100). Journal of Physical Chemistry C, 2022, 126, 10035-10044.	3.1	7
344	Direct Observation of Nanoscale Native Oxide on 6H-SiC Surface and Its Effect on the Surface Band Bending. Applied Physics Express, 2012, 5, 105802.	2.4	6
345	Growth and Electronic Properties of Ag Nanoparticles on Reduced CeO2â^' <i>x</i> (111) Films. Chinese Journal of Chemical Physics, 2012, 25, 713-718.	1.3	6
346	Calcium Thin Film Growth on Polyfluorenes: Interface Structure and Energetics. Journal of Physical Chemistry C, 2014, 118, 2953-2962.	3.1	6
347	Interaction of cobalt with ceria thin films and its influence on supported Au nanoparticles. Chinese Chemical Letters, 2017, 28, 1760-1766.	9.0	6
348	Controlling the Topology of Low-Dimensional Organic Nanostructures with Surface Templates. Wuli Huaxue Xuebao/ Acta Physico - Chimica Sinica, 2017, 33, 1288-1296.	4.9	6
349	Co-precipitation synthesis of reusable ZnAl-CLDH/ZIF-8 heterojunction for enhanced photodegradation of organic dye. Journal of Materials Science: Materials in Electronics, 2021, 32, 28051-28064.	2.2	6
350	Sequential Activation of Aromatic C─H Bonds on Cu(111). Journal of Physical Chemistry C, 2022, 126, 5541-5549.	3.1	6
351	Regulating Electronic Structure in Bi ₂ O ₃ Architectures by Ti Mediation: A Strategy for Dual Active Sites Synergistically Promoting Photocatalytic Nitrogen Hydrogenation. ChemSusChem, 2022, 15, .	6.8	6
352	Experimental determination of valence band offset at PbTe/Ge(100) interface by synchrotron radiation photoelectron spectroscopy. Applied Surface Science, 2010, 256, 6057-6059.	6.1	5
353	Atomic-Scale Insight into the Metal–Support Interaction: A Case for Ag Nanoparticles on Ordered ZrO ₂ (111) Thin Films. Journal of Physical Chemistry C, 2015, 119, 4235-4241.	3.1	5
354	On-Surface Synthesis of a Five-Membered Carbon Ring from a Terminal Alkynyl Bromide: A [4 + 1] Annulation. Journal of Physical Chemistry Letters, 2020, 11, 5902-5907.	4.6	5
355	Defects controlled doping and electrical transport in TiS2 single crystals. Applied Physics Letters, 2020, 116, .	3.3	5
356	Lateral Modulation of Magnetic Anisotropy in Tricolor 3d–5d Oxide Superlattices. ACS Applied Electronic Materials, 2021, 3, 4210-4217.	4.3	5
357	Structure and properties of samarium overlayer and Sm/Rh surface alloy on Rh(100). Science Bulletin, 2001, 46, 1689-1691.	1.7	4
358	X-Ray Magnetic Circular Dichroism Measurement of Fe–Co Alloy Films Prepared by Electrodeposition. Chinese Physics Letters, 2007, 24, 2667-2670.	3.3	4
359	Study of 5d6s valence band and 4f states for metal Sm by synchrotron radiation photoelectron spectroscopy. Surface Science, 2008, 602, 3728-3732.	1.9	4
360	Adsorption of water molecules on the CdZnTe (111) B surface. Chemical Physics Letters, 2010, 489, 103-106.	2.6	4

#	Article	IF	CITATIONS
361	Photoemission intensity oscillations in the valence bands of C70 film. Journal of Electron Spectroscopy and Related Phenomena, 2011, 184, 414-419.	1.7	4
362	Performance of the undulator based ultraviolet and soft x-ray beamline for catalysis and surface science at National Synchrotron Radiation Laboratory. Nuclear Instruments and Methods in Physics Research, Section A: Accelerators, Spectrometers, Detectors and Associated Equipment, 2016, 838, 62-65.	1.6	4
363	Interface properties between a low band gap conjugated polymer and a calcium metal electrode. Physical Chemistry Chemical Physics, 2016, 18, 9446-9452.	2.8	4
364	Electronic states of Ca/PC61BM: Mechanism of low work function metal as interfacial material. AIP Advances, 2018, 8, 035015.	1.3	4
365	Photocatalytic fixation of nitrogen to ammonia by NiFe-LDH-derived sulfide microspheres. Journal of Materials Science: Materials in Electronics, 2021, 32, 13396-13408.	2.2	4
366	Valence photoemission intensity oscillations of C84. Carbon, 2012, 50, 1762-1768.	10.3	3
367	Electronic properties of aluminum/CdZnTe interfaces. Applied Physics Letters, 2013, 102, 211602.	3.3	3
368	Low-Temperature Growth Improves Metal/Polymer Interfaces: Vapor-Deposited Ca on PMMA. Journal of Physical Chemistry C, 2014, 118, 6352-6358.	3.1	3
369	Mechanism of Low Schottky Barrier Formation for Chromium/CdZnTe Contact. Journal of Physical Chemistry C, 2014, 118, 5294-5298.	3.1	3
370	Purine on graphene: PES and NEXAFS study of a heterocyclic aromatic organic compound. Current Applied Physics, 2016, 16, 1120-1123.	2.4	3
371	Effects of Ga–Te interface layer on the potential barrier height of CdTe/GaAs heterointerface. Physical Chemistry Chemical Physics, 2016, 18, 2639-2645.	2.8	3
372	An ultrathin cuprite film on Pt(111) with high reactivity to CO. Chemical Communications, 2019, 55, 5825-5828.	4.1	3
373	Direct on-surface synthesis of gold–phthalocyanine <i>via</i> cyclization of cyano-groups with gold adatoms. Materials Chemistry Frontiers, 2019, 3, 1406-1410.	5.9	3
374	Surface-mediated ordering of pristine Salen molecules on coinage metals. Inorganic Chemistry Frontiers, 2021, 8, 417-424.	6.0	3
375	Osmotic pressure-induced pocket-like spheres with Fe single-atom sites for the oxygen reduction reaction. Journal of Materials Chemistry A, 2021, 9, 13908-13915.	10.3	3
376	Fluorination-Guided Li-Anchoring Behaviors on Phthalocyanines. Journal of Physical Chemistry C, 2021, 125, 8236-8243.	3.1	3
377	Strongly Coupled Cobalt Diselenide Monolayers Selectively Catalyze Oxygen Reduction to H2O2 in an Acidic Environment. Angewandte Chemie, 0, , .	2.0	3
378	Role of Interfaces in the Thermal Reduction Process of the FeO/Cu2O/Cu(100) Surface. Journal of Physical Chemistry C, 2021, 125, 20863-20869.	3.1	3

#	Article	IF	CITATIONS
379	Bismuth sulfide bridged Bi2S3/sulfuretted ZnAl-LDHs heterojunctions for synergetic enhancement of photodegradation activity towards tetracycline degradation. Journal of Materials Science: Materials in Electronics, 2022, 33, 871-883.	2.2	3
380	Photoemission study on the growth and stability of Gd cluster films over Ni(110) surface. Journal of Electron Spectroscopy and Related Phenomena, 2001, 114-116, 533-537.	1.7	2
381	Effects of dispersant on performance of Ni-Zn batteries. Central South University, 2010, 17, 930-935.	0.5	2
382	Electronic structure of Eu–C ₇₀ fullerides. Journal of Physics Condensed Matter, 2010, 22, 175504.	1.8	2
383	In-Situ SRPES Study on the Band Alignment of (0001)CdS/CdTe Heterojunction. Chinese Physics Letters, 2012, 29, 057301.	3.3	2
384	Effect of Ar+ ion etching treatment on the surface work function of Hg3ln2Te6 wafer. Journal of Electron Spectroscopy and Related Phenomena, 2013, 187, 49-52.	1.7	2
385	Probing substrate-induced perturbations on the band structure of graphene on Ni(1 1 1) by soft X-ray emission spectroscopy. Chemical Physics Letters, 2013, 580, 43-47.	2.6	2
386	Electronic States of IC ₆₀ BA and PC ₇₁ BM. Chinese Physics Letters, 2013, 30, 117103.	3.3	2
387	Design of a Varied-line-spacing plane grating monochromator at NSRL for surface physics experiments. Journal of Physics: Conference Series, 2013, 425, 162008.	0.4	2
388	Novel Core-Shell Nanoparticle@Metal-Organic Framework Composite Materials as Heterogeneous Catalysts. , 2017, , 229-248.		2
389	On‣urface Synthesis. ChemPhysChem, 2019, 20, 2249-2250.	2.1	2
390	Morphologies and Electronic Structures of Calcium-Doped Ceria Model Catalysts and Their Interaction with CO ₂ . Wuli Huaxue Xuebao/ Acta Physico - Chimica Sinica, 2018, 34, 1381-1389.	4.9	2
391	Surface morphology of F8BT films and interface structures and reactions of Al on F8BT films. Wuli Xuebao/Acta Physica Sinica, 2015, 64, 077304.	0.5	2
392	Application of confinement effects in on-surface chemistry. Scientia Sinica Chimica, 2019, 49, 516-524.	0.4	2
393	Adsorption and reaction of an alkyne molecule on diverse oxygen-reconstructed Cu(110) surfaces. Surface Science, 2022, 719, 122039.	1.9	2
394	Converting <i>n</i> -Alkanol to Conjugated Polyenal on Cu(110) Surface at Mild Temperature. Journal of Physical Chemistry Letters, 2022, , 3276-3282.	4.6	2
395	Band Mapping of Graphene Studied by Resonant Inelastic X-ray Scattering. Fullerenes Nanotubes and Carbon Nanostructures, 2015, 23, 471-475.	2.1	1
396	Band offsets of ZnO/PbTe heterostructure determined by synchrotron radiation photoelectron spectroscopy. Wuli Xuebao/Acta Physica Sinica, 2014, 63, 167301.	0.5	1

#	Article	IF	CITATIONS
397	Synchrotron radiation photoemission study on growth of gadolinium film over Ni(110) surface. Science Bulletin, 1999, 44, 328-331.	1.7	0
398	Oxidation of Gd–Ni composite and Gd cluster films grown on Ni(110) surface studied by photoemission. Journal of Electron Spectroscopy and Related Phenomena, 2001, 114-116, 357-361.	1.7	0
399	Preparation and properties of the SmOx/Rh(100) model surface. Science Bulletin, 2002, 47, 1184-1186.	1.7	0
400	Alignment of the photoelectron spectroscopy beamline at NSRL. Chinese Physics C, 2013, 37, 118002.	3.7	0
401	THE ADSORPTION AND DESORPTION OF OXYGEN ON CdZnTe (111) B -(2 × 2) SURFACE. Surface Review and Letters, 2013, 20, 1320001.	1.1	0
402	Growth and Interfacial Interaction of Cu on ZrO ₂ (111) Thin Film. Chinese Journal of Catalysis, 2013, 33, 1712-1716.	14.0	0
403	Growth, Electronic Structure and Thermal Stability of Ni on ZrO ₂ (111) Thin Film Surfaces. Wuli Huaxue Xuebao/ Acta Physico - Chimica Sinica, 2015, 31, 2151-2157.	4.9	0
404	Binodal Organometallic Network Achieved by On-Surface Dissymmetric Reaction. Wuli Huaxue Xuebao/ Acta Physico - Chimica Sinica, 2019, 35, 1297-1298.	4.9	0
405	Charged Exciton Formation in Compact Polycrystalline Perovskite Thin Films. ACS Photonics, 2022, 9, 1614-1620.	6.6	0
406	Selective CO2 Photoreduction to CH4 via Pdᵟ+â€assisted Hydrodeoxygenation over CeO2 Nanosheets. Angewandte Chemie, 0, , .	2.0	0